Hindawi
International Journal of Antennas and Propagation
Volume 2024, Article ID 5761698, 15 pages
https://doi.org/10.1155/2024/5761698

Research Article

Design of the Monopulse Feeding Network for a Slotted Waveguide Array on an Annular Disk

Zongxin Wang, Yulan Wang, Shengchi Zhu, and Peng Chen

State Key Laboratory of Millimeter Waves, Southeast University, Nanjing 210096, China

Correspondence should be addressed to Zongxin Wang; wangzx@seu.edu.cn

Received 10 January 2024; Revised 20 February 2024; Accepted 22 March 2024; Published 16 April 2024

Academic Editor: Mohammad Hassan Neshati

Design of a monopulse feeding network including a compact power distribution network and a monopulse comparator for a dual polarization slotted waveguide array fabricated on an annular disk is presented in this paper. As the slotted waveguide array is arranged on an annular disk, the feeding network is more complicated than that of a regular array such as a rectangular array. The design details of some key waveguide components, such as the compact assembly of H-plane T-junctions and E-plane elbows used to connect power distribution networks and radiation waveguides, are provided. Quasiplanar magic tees are designed and used to construct the compact sum and difference comparator. The antenna system contains two comparators, which are used to generate sum and difference beams for horizontal polarization and vertical polarization, respectively. Finally, the monopulse slotted waveguide array antenna is divided into two modules, a comparator module and an antenna module (including power distribution network), and fabricated with the layered processing and bonding process. The comparator module is measured using a network analyzer to verify its amplitude-frequency characteristics and phase-frequency characteristics. Screwing the comparator module and the antenna module together, a monopulse slotted waveguide array antenna is obtained, and the sum beam and difference beam characteristics of the antenna are measured in a microwave chamber and presented.

1. Introduction

A tracking radar is widely used not only in military departments, such as fire control of weapons and missile guidance, but also in civil fields, such as satellite tracking [1] and meteorology [2]. If the measurement is not based on one pulse but on multiple pulses, the amplitude fluctuations between the echo pulses will affect the tracking accuracy [3]. A radar system that can provide angle error information with only one echo pulse is called a monopulse (or simultaneous lobing) radar. In a monopulse radar system, the antenna must generate more than one receiving beam. By comparing the relative amplitude or phase of different beams, the angle of the echo signal (i.e., the angle of the target) can be obtained. Based on two receiving beams, only a single plane's angle error information can be obtained. Therefore, in order to achieve two-dimensional tracking of the target, which involves obtaining both azimuth and elevation angle error information, four antenna beams are required.

The antenna forms of monopulse tracking systems mainly include reflector antennas, slotted waveguide antennas (SWAs), and microstrip patch array antennas. Due to significant feed line losses [4–7], especially at high frequencies, microstrip patch antenna arrays are mainly used in low-frequency systems. Both the reflector antenna and SWA can be fed using waveguide-based feeding networks to fully utilize the low loss characteristics of waveguides. Reflector antennas are three-dimensional structures, which are usually larger in size. The SWAs, on the other hand, are planar structures, which are compact and reliable, making them more suitable in space limited platforms, such as certain aircraft, than the reflector antennas [8]. In a SWA monopulse antenna, the antenna aperture is usually divided into four quadrants. Each quadrant contains a slotted waveguide subarray, which is fed by a power distribution feeding network (PDFN). Four subarrays are connected to a comparator network to provide the sum (carrying distance information), the

azimuth difference (carrying azimuth angle information), and the elevation difference (carrying pitch angle information) signals. The comparator contains four hybrids (magic tees or equivalent), and this is similar to most comparators for two-dimensional monopulse tracking antennas [9–11]. Here, the PDFN (feeding the subarray) and the comparator are collectively referred to as a monopulse feeding network (MFN).

A design of the W-band dual polarized SWA on an annular disk has been presented in our previous paper [12], which focuses on the arrangement of rectangular waveguides and ridge waveguides in limited space, the layout of two polarization slots on a circular disk, and the optimization method of the slot parameters, and so the design details of the PDFN for feeding the SWA are not specifically introduced. In this paper, an irregular PDFN (composed of several key waveguide components) adapted to the slotted waveguide array arranged on the annular disk will be given, and more importantly, the design of two comparators (for two different polarizations) adapted to the SWA designed will be presented. The comparators are compact in terms of height as they are designed based on a kind of quasiplanar magic tee [13]. The MFN composed of the power distribution network and the comparator is then integrated with the SWA to obtain the final dual polarization monopulse SWA.

2. Design of the Monopulse Feeding Network

2.1. Design of the Power Distribution Network. The slotted waveguide array to be fed has two characteristics: orthogonal dual polarization and annular aperture. To provide the orthogonal dual polarization, the combination of two separate waveguide arrays of vertical polarization (VP) and horizontal polarization (HP) is usually used. Many building blocks have been reported [14–16] in the C-band and X-band where the slotted waveguide and feeding structures are relatively easy to process. However, those structures are no longer applicable in the W-band due to fabrication difficulties. In our design, a broad wall longitudinal offset slot array and an edge wall inclined slot array [12] are used to provide HP and VP, respectively. The typical feeding method of the slotted waveguide array is shown in Figure 1, where the feeding waveguide is placed under the radiating waveguide array and distributes power though the coupling slots cut in the shared wall of the radiating waveguide and feeding waveguide.

This feeding technique is no longer applicable to our design due to two reasons: (a) the antenna aperture is circular so the ends of all the radiating waveguides are not able to arrange in a straight line and (b) the bottom walls of the ridged waveguides of the HP array and the side walls of the rectangular waveguides of the VP array are not wide enough, so the coupling slots cut in those walls cannot provide enough coupling to the feeding waveguide.

One quadrant of the annular SWA of our design is shown in Figure 2, where Figure 2(a) is the front of the SWA, Figure 2(b) is the two PDFNs (for dual polarizations) on the back of the array, and Figure 2(c) is the 3D view of the interconnection between the feed network and the radiation waveguide. The HP slots and VP slots are cut on a thin metal layer covering the HP radiation waveguides and VP radiation waveguides, respectively. The layout of the PDFN is determined by the radiation waveguides distributed along the annular disk and the stacking and interconnection details of the radiation waveguide and two PDFNs can be found in Figure 2(c), where a local part of the VP feeding network is cut open (see the dashed frame) to display the connection detail of the HP feeding network and the HP radiation waveguides. The HP waveguides are bent and transformed to rectangular waveguides placed at the back of the array and then connected to a waveguide power divider network. For the sake of clarity, only the waveguide air cavities (without metal wall) are given in Figures 2(b) and 2(c). In the VP array, every two adjacent waveguides are combined through waveguide bends to an H-plane T-junction (TH in Figure 2(c)) firstly and then bend the main arm of T-junction to the back of the array and connected to a waveguide power divider network.

For clarity, the PDFNs of HP and VP are pulled out, as shown in Figures 3 and 4, respectively. Key waveguide components of the PDFN to be discussed here include a compact 1 to 4 power divider (as in the dashed box enlarged and placed in the upper right corner in Figure 3), a rectangular waveguide to ridged waveguide transition bend (as in the dashed box enlarged and placed in the upper left corner in Figure 3), and a compact assembly of 1 to 2 power divider and E-plane waveguide bends (as in the dashed box enlarged and placed in the upper right corner in Figure 4). The orange parts of Figures 3 and 4 are identical PDFN, which is an unequal power distribution network that includes three unequal power dividers T1, T2, and T3. The electromagnetic wave amplitude along the diameter of an annular array should be evenly distributed to obtain good side lobe characteristics. Therefore, the power distribution ratio of T1, T2, and T3 must be 4 : 7 (where the meaning of 4 : 7 is that the ratio of power distributed to two subports is 4 to 7), 3 : 4, and 1 : 2, respectively, to enable each radiating waveguide obtaining the same power. On the other hand, it is necessary to ensure that the waves arriving at all subport are in phase, i.e., all the wave path lengths from main port P1 to all subports must be equal.

2.1.1. Compact 1 to 4 Power Divider of HP PDFN. Due to the dense arrangement of the radiation waveguide array, the space for the associated PDFN is also very small.

In particular, a compact 1 to 4 power divider for the HP waveguide array is required. Generally, a 1 to 4 power divider can be composed of three identical 3 dB power dividers, and the input ports of the two secondary-stage 3 dB power dividers are connected to the output ports of the first-stage 3 dB power dividers. However, the connection waveguide of the two-stage 3 dB power divider needs to be relatively long so that the first and second stages do not interfere with each other. In our design, there are many matching steps and wedges, and all matching structures of this compact 1 to 4 power divider need unified parameter

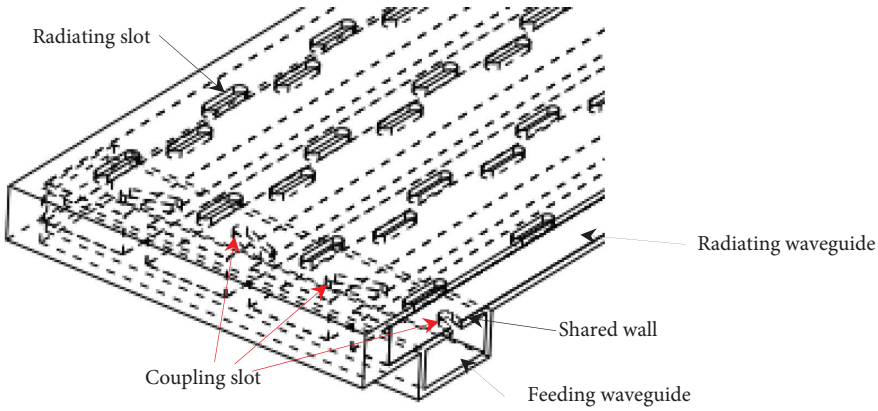

Figure 1: Typical feeding method of the slotted waveguide array.

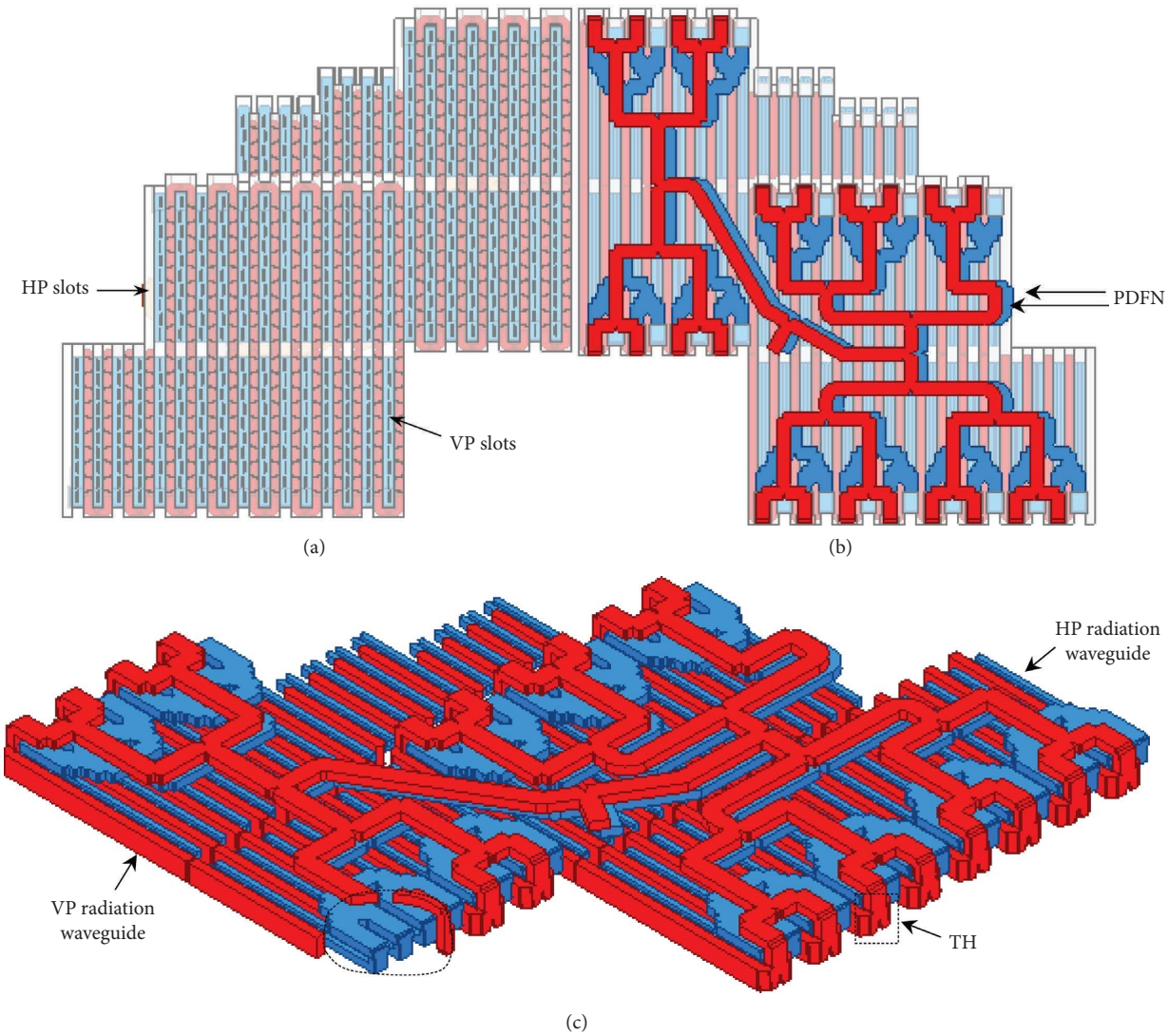

Figure 2: Dual polarization SWA and PDFN: (a) front of the slotted waveguide array, (b) feeding network on the back, and (c) 3D view of the interconnection between the feed network and the radiation waveguide.

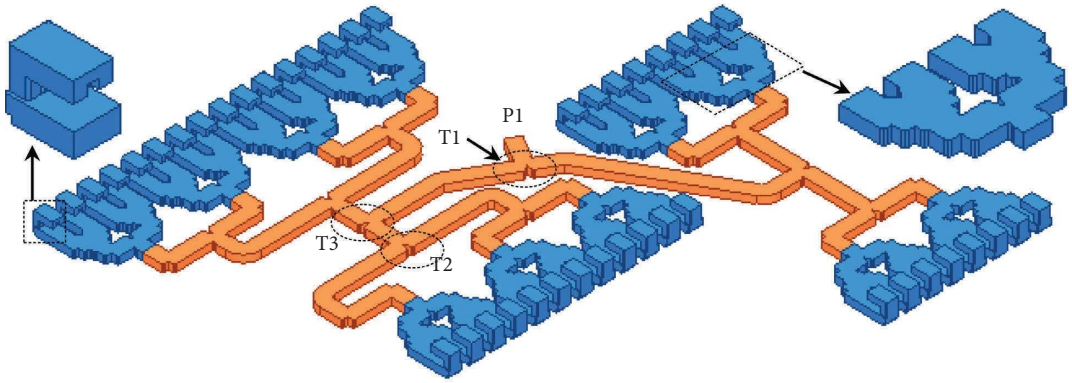

Figure 3: PDFN of horizontal polarization.

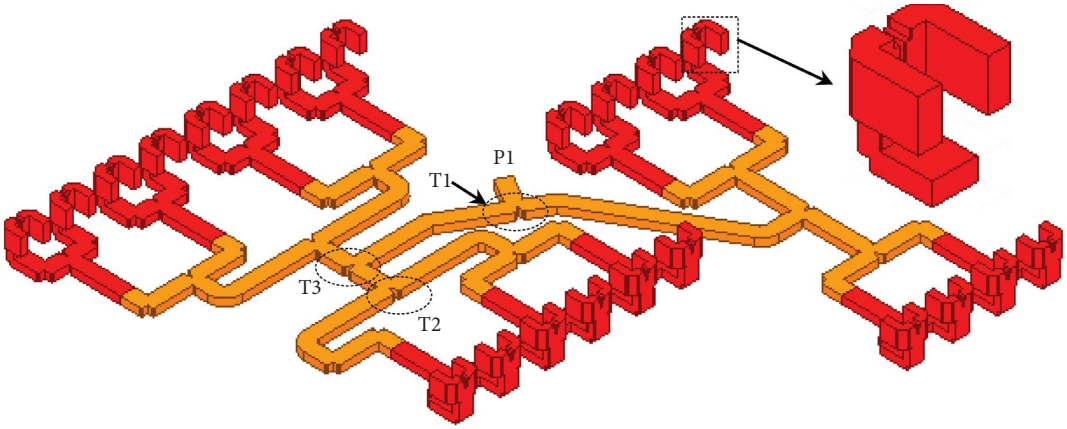

Figure 4: PDFN of vertical polarization.

optimization. The 1 to 4 power divider (with a central operating frequency f_0 of 94.7 GHz) is finally designed based on a rectangular waveguide of $0.627\lambda_0 \times 0.3135\lambda_0$ (width × height, λ_0 is the center frequency wavelength of free space); the designed 1 to 4 power divider is shown in Figure 5(a), the optimized structural parameters of the power divider are given in Table 1, and the corners of the steps have been chamfered (chamfer radius is $0.078\lambda_0$) for ease of machine processing. The simulated results are given in Figure 5(b); it can be seen that the power input from port 1 is approximately distributed evenly to ports 2~5, and the reflection coefficient of port 1 is less than −30 dB.

2.1.2. Rectangular Waveguide to Ridged Waveguide Transition Bend of HP PDFN. A ridged waveguide, which has smaller width than the rectangular waveguide, is used to form the HP slotted radiation waveguide array to save space. The ridged radiation waveguide should be connected to the feeding rectangular waveguide through a waveguide bend transition, as shown in Figure 6(a).

The main match structure is a corner step, and by optimization of two parameters c_1 and c_2 of the step and the length c_3 of the connecting waveguide, it is easy to obtain a bend transition with good transmission characteristics. The final optimized parameters are given in Table 2, and the simulated transmission and reflection results of the final optimized waveguide bends are given in Figure 6(b); the reflection coefficient is less than −20 dB in a 10% frequency bandwidth.

2.1.3. Compact Assembly of 1 to 2 Power Divider and E-Plane Waveguide Bend of VP PDFN. In addition to small space, a compact assembly of a 1 to 2 power divider and waveguide E-plane bend is required for connecting VP radiation waveguides and PDFN. The assembly consists of an H-plane T and three E-plane bends. As shown in Figure 7(a), many matching structures, including corner steps, stepped gaps, and chamfers, are used to obtain good transmission characteristics. Optimized parameters of these matching structures are given in Table 3. The simulation results of the assembly are given in Figure 7(b); the reflection parameters are better than −33 dB, and the power is evenly distributed to ports 2 and 3.

2.1.4. Design of 4 : 7 Unequal Power Divider. As described in Section II-A, the design of a 4 : 7 power divider will be given here as a representative of the unequal power distributor. The structural details and simulation results of the 4 : 7 power divider are shown in Figures 8 and 9.

Structure parameters of the 4 : 7 power divider are given in Table 4. It can be seen from Figure 9(a) that the return loss is better than −35 dB, and the transmission

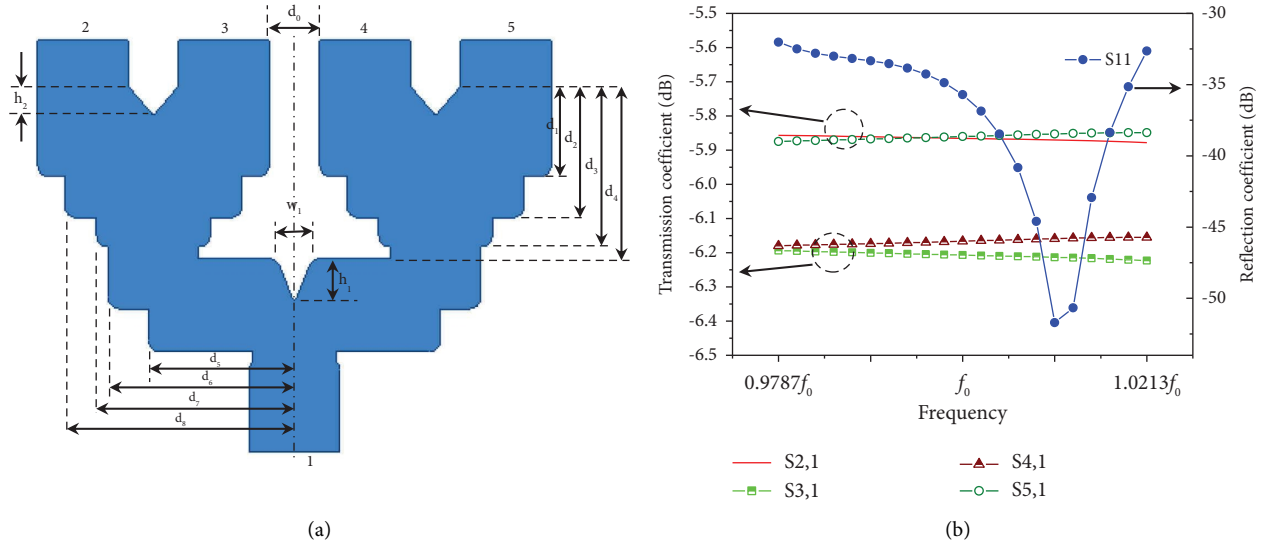

Figure 5: 1 to 4 power divider: (a) structural diagram and (b) simulated scattering parameters.

Table 1: Structural parameters of the 1 to 4 power divider.

d_0	d_1	d_2	d_3	d_4	d_5	d_6	d_7	d_8	w_1	h_1	h_2
$0.351\lambda_0$	$0.63\lambda_0$	$0.915\lambda_0$	$1.12\lambda_0$	$1.2\lambda_0$	$1.012\lambda_0$	$1.291\lambda_0$	$1.371\lambda_0$	$1.592\lambda_0$	$0.242\lambda_0$	$0.31\lambda_0$	$0.21\lambda_0$

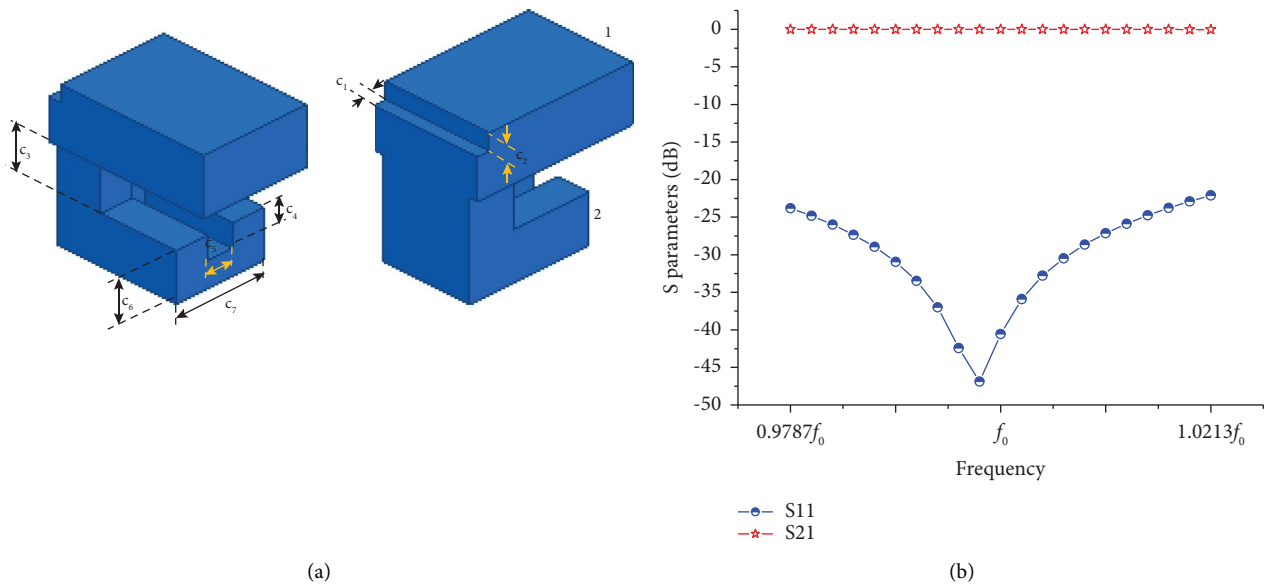

Figure 6: Rectangular waveguide to ridged waveguide transition bend: (a) structural diagram and (b) simulated scattering parameters.

Table 2: Structural parameters of the rectangular waveguide to ridged waveguide transition bend.

c_1	c_2	c_3	c_4	c_5	c_6	c_7
$0.07\lambda_0$	$0.09\lambda_0$	$0.266\lambda_0$	$0.13\lambda_0$	$0.15\lambda_0$	$0.27\lambda_0$	$0.53\lambda_0$

coefficients S21 and S31 are −4.4 dB and −2 dB, respectively, meeting the power allocation ratio of 4 : 7. The phase-frequency characteristics of the electromagnetic signals of port 2 and port 3 are also given in Figure 9(b), indicating that the signals of the two ports are basically in phase.

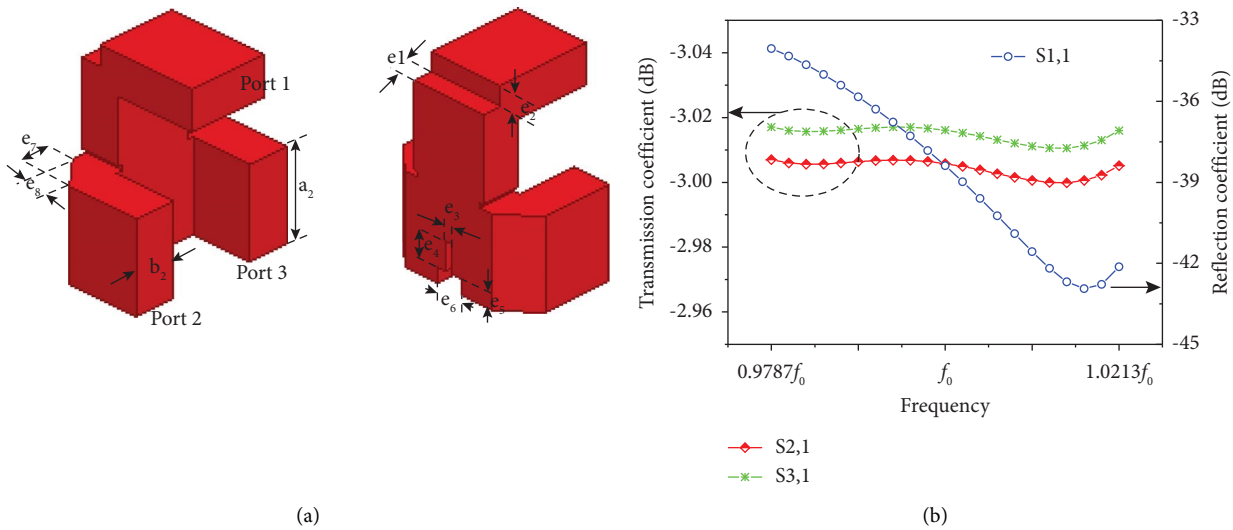

Figure 7: Compact assembly of the 1 to 2 power divider and E-plane waveguide bend: (a) structural diagram and (b) simulated scattering parameters.

Table 3: Structural parameters of assembly of 1 to 2 power divider and E-plane waveguide bend.

e_1	e_2	e_3	e_4	e_5	e_6	e_7	e_8	a_2	b_1
$0.154\lambda_0$	$0.154\lambda_0$	$0.062\lambda_0$	$0.227\lambda_0$	$0.12\lambda_0$	$0.22\lambda_0$	$0.255\lambda_0$	$0.23\lambda_0$	$0.71\lambda_0$	$0.32\lambda_0$

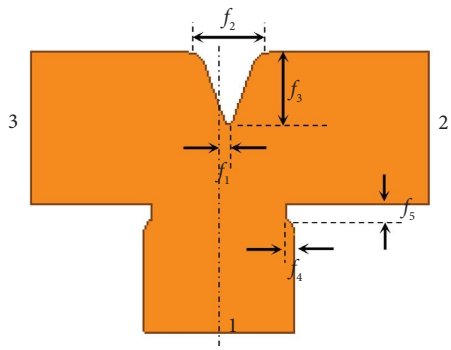

Figure 8: Structural details of the 4 : 7 power divider.

2.1.5. Overall Performance of the VP PDFN. After the design of the key waveguide components mentioned above is completed, the PDFN can be formed through these components and some necessary waveguide connectors such as the 3 dB waveguide power divider and waveguide bend, and it is necessary to ensure that all path lengths from port 1 to other ports are equal. Here, we only give the simulation results of the overall structure of VP PDFN; the overall characteristics of the HP PDFN are similar. The port number of the network is shown in Figure 10(a), and the simulated amplitude-frequency characteristics and phase-frequency characteristics of the scattering parameters are shown in Figures 10(b) and 10(c), respectively. The reflection coefficient is less than −25 dB at most frequencies, and the power is basically evenly distributed to each subport. It should be noted from Figure 10(c) that the phases of neighboring output ports are out of phase, and this means that adjacent radiation waveguides of the VP array are excited by polarization inverted electromagnetic waves, so the slots of the VP antenna must be so designed that the slot inclination directions at the same positions of two adjacent waveguides must be opposite to each other, see Figure 2(a).

2.2. Design of the Sum and Difference Network. As known to all, to generate sum and difference beams for a monopulse system, a comparator network is required. Because there are two types of slot arrays (with orthogonal polarization) in our design, two comparator networks are needed, which are connected separately to the VP array and HP array to generate their respective sum and difference beams. The key component of the comparator network is the quasiplanar magic tee (QPMT) shown in Figure 11. Compared with the traditional magic tee, the QPMT is compact and easy to be fabricated with the layered processing and bonding process. The QPMT is composed of an H-plane tee junction (HTJ),

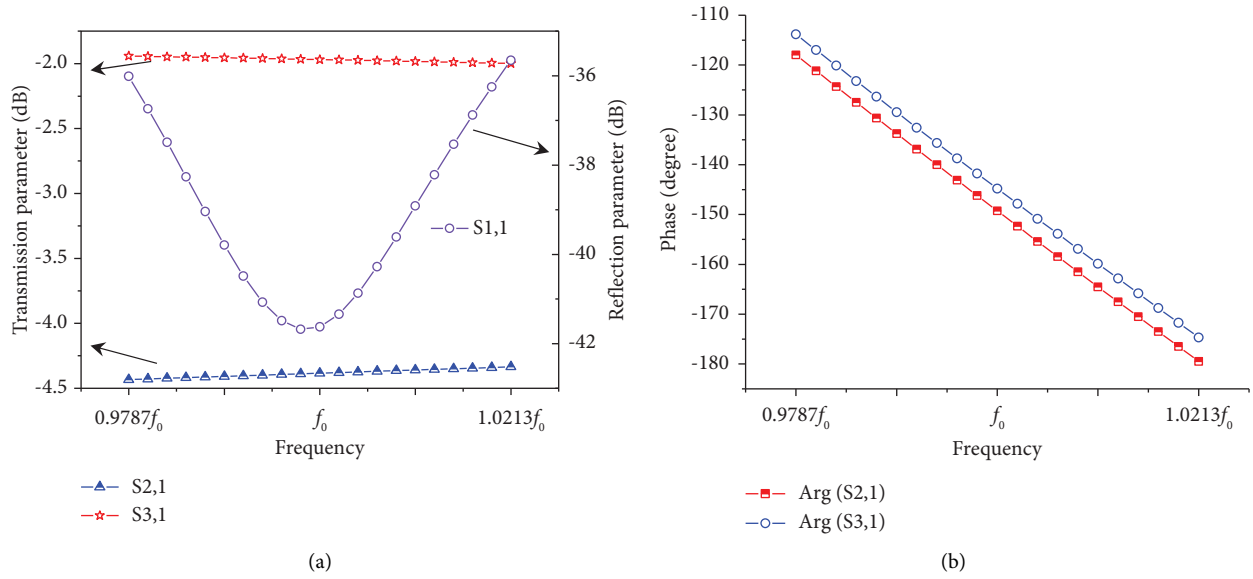

Figure 9: Simulated results of the 4 : 7 power divider: (a) scattering parameters and (b) phase-frequency characteristics.

Table 4: Structure parameters of the 4:7 power divider.

f_1	f_2	f_3	f_4	f_5
$0.038\lambda_0$	$0.238\lambda_0$	$0.33\lambda_0$	$0.035\lambda_0$	$0.063\lambda_0$

a waveguide, and a coupling hole. The waveguide is offset on one side of the main arm axis of the HTJ and connected with the HTJ through the coupling hole. The HTJ has a slot for impedance matching. The simulated results of the optimized QPMT are shown in Figure 12. It can be seen that when incident at port 1, the input power is divided equally and in phase to ports 2 and 3, see Figure 12(a), and when incident at port 2, the input power is divided equally and out of phase to ports 2 and 3, see Figure 12(b). The reflection and isolation characteristic curves are better than 20 dB; see Figure 12(c).

Based on four QPMTs (enclosed in the dashed circle in Figure 13), a comparator for the VP array is designed and shown in Figure 13. The comparator for the HP array is similar and not given any more. The reason why the comparator is designed in this shape is to match the dual polarization array on the annular disk. A split structure diagram shown in Figure 14 is used to illustrate the spatial layout relationship between the radiation waveguide array, the PDFN, and the sum and difference comparator, and for clarity, only one quadrant of the waveguide array and its PDFN is shown.

Referring to Figure 13, the small arrows at ports 1, 2, 3, and 4 represent the integration line direction of the waveguide port set in HFSS. Let us use ports 1 and 4 to explain why the integration line directions are set in this way. When incident at port Sum, electromagnetic waves reached at ports 1 and 4 are out of phase because ports 1 and 4 are separately connected with the E-plane elbows and the two elbows bent 90° in the opposite direction. Therefore, the integration line directions at ports 1 and 4 are set to be opposite to each other. Waveguide ports marked as Sum, Az., Pit., and Idle are sum beam port, azimuth difference beam port, pitch difference beam port, and idle port (connected to a matching load and not used), respectively. The simulated results of the comparator are shown in Figure 15. It can be seen from Figures 15(a)–15(c) that when incident at ports Sum, Az., and Pit., respectively, electromagnetic waves are almost evenly distributed (standard value -6.02 dB) to ports 1, 2, 3, and 4. When incident at port Sum, all the distributed electromagnetic wave signals at ports 1~4 are in phase; when incident at ports Az., ports 1 and 4 are in phase and ports 2 and 3 are also in phase, but ports 1 and 2 are out of phase (ports 3 and 4 are also out of phase, of course); and when incident at port Pit., ports 1 and 2 are in phase and ports 3 and 4 are also in phase, but ports 1 and 3 (or ports 2 and 4) are out of phase. The amplitude and phase relationship between the ports described above shows that the comparator we designed is a good sum and difference beamforming network. Typical port reflection coefficients of the comparator are given in Figure 15(d), nearly −20 dB in the most frequency band.

3. Fabrication and Measurement

Finally, the monopulse SWA is divided into two modules for easy processing and testing, a comparator module and an antenna module (including SWA and PDFN). The comparator model established in structural design software is shown in Figure 16, and the antenna module has been described in detail in [12] and will not be given again here. The two modules are fabricated with the layered processing and bonding process. During the processing, every model is divided into several thin aluminum alloy layers from the top to bottom, which are separately milled out in the machining center and then laminated and diffusion bonded together. The manufactured MFN prototype is shown in Figure 17.

The waveguide port of the prototype is not a standard waveguide port, and the distance between adjacent ports is too close, so it must be connected to the standard

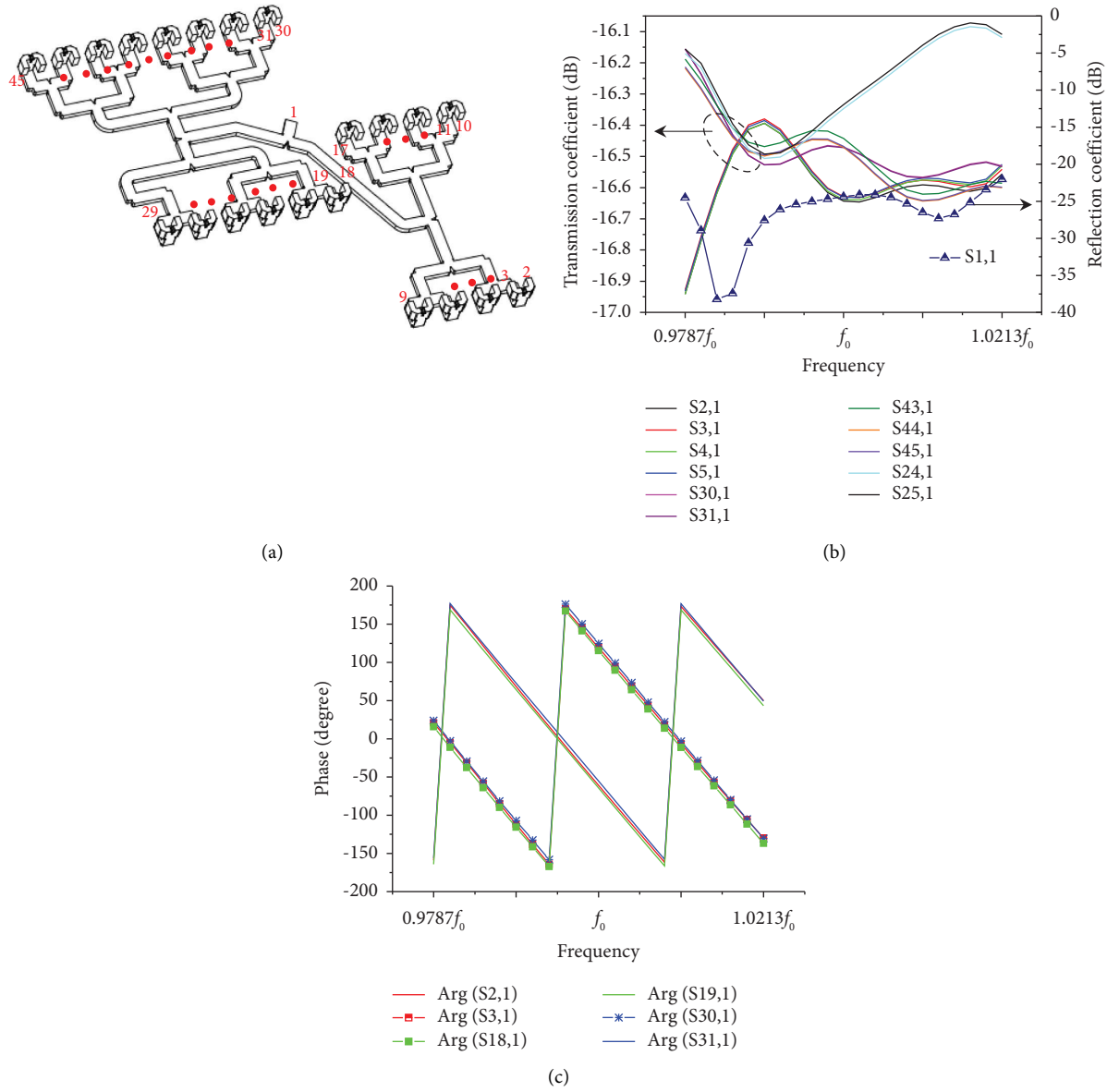

FIGURE 10: Simulated results of VP PDFN: (a) port number, (b) amplitude-frequency characteristics of the VP PDFN, and (c) phase-frequency characteristics of the VP PDFN.

waveguide port of the network analyzer through a transition during testing; see Figure 18. The measured results of the comparator are shown in Figure 19, and it can be seen from Figures 19(a)–19(c) that when incident at ports Sum, Az., and Pit., respectively, the power distributed to ports 1~4 is approximately −6.8 dB each, and this value is 0.8 dB lower than that of the simulated results, which is supposed to be caused by the conductor loss of the waveguide. The in-phase or out-phase pattern of the measured results is consistent with the simulation results; however, due to the inclusion of transitions in the measuring, the length of the channel is increased, so the phase values in the simulation and test results are different. Port reflection coefficients of the comparator are given in Figure 19(d), better than −15 dB in the most frequency band.

In our previous paper [12], we presented a fabricated SWA. Due to the fine structure in the W-band, it is very difficult to process the waveguide slot, and the VP array is slightly damaged locally; see the area enclosed in the red dotted box in Figure 20(a). The antenna has been reprocessed and has not suffered any damage this time; see Figure 20(b). Then, by screwing the comparator and SWA together, a monopulse SWA is obtained. Radiation patterns of the monopulse antenna are measured in a microwave chamber. The measured sum and difference patterns at the center frequency f_0 are given in Figure 21. The measured sum beam gains of the HP and VP are 35.9dBi and 35.6dBi, respectively, and the sum beam side lobe levels (SLLs) of HP and VP are −10.5 dB and −10 dB, respectively, and the 3dB sum beam widths of HP and VP are both 1.2°; see Figures 21(a) and 21(b). The antenna we designed is used for

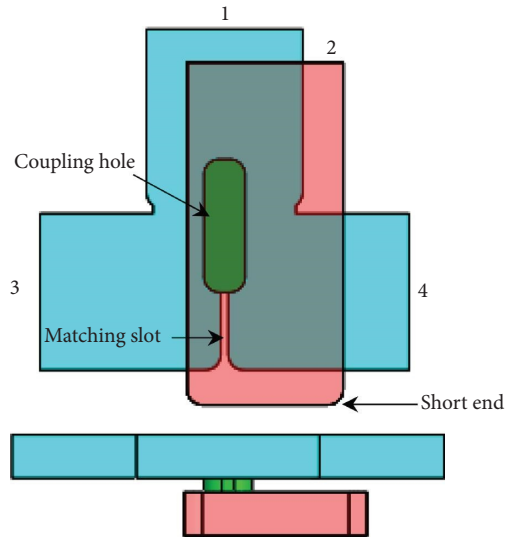

Figure 11: Structure of the QPMT.

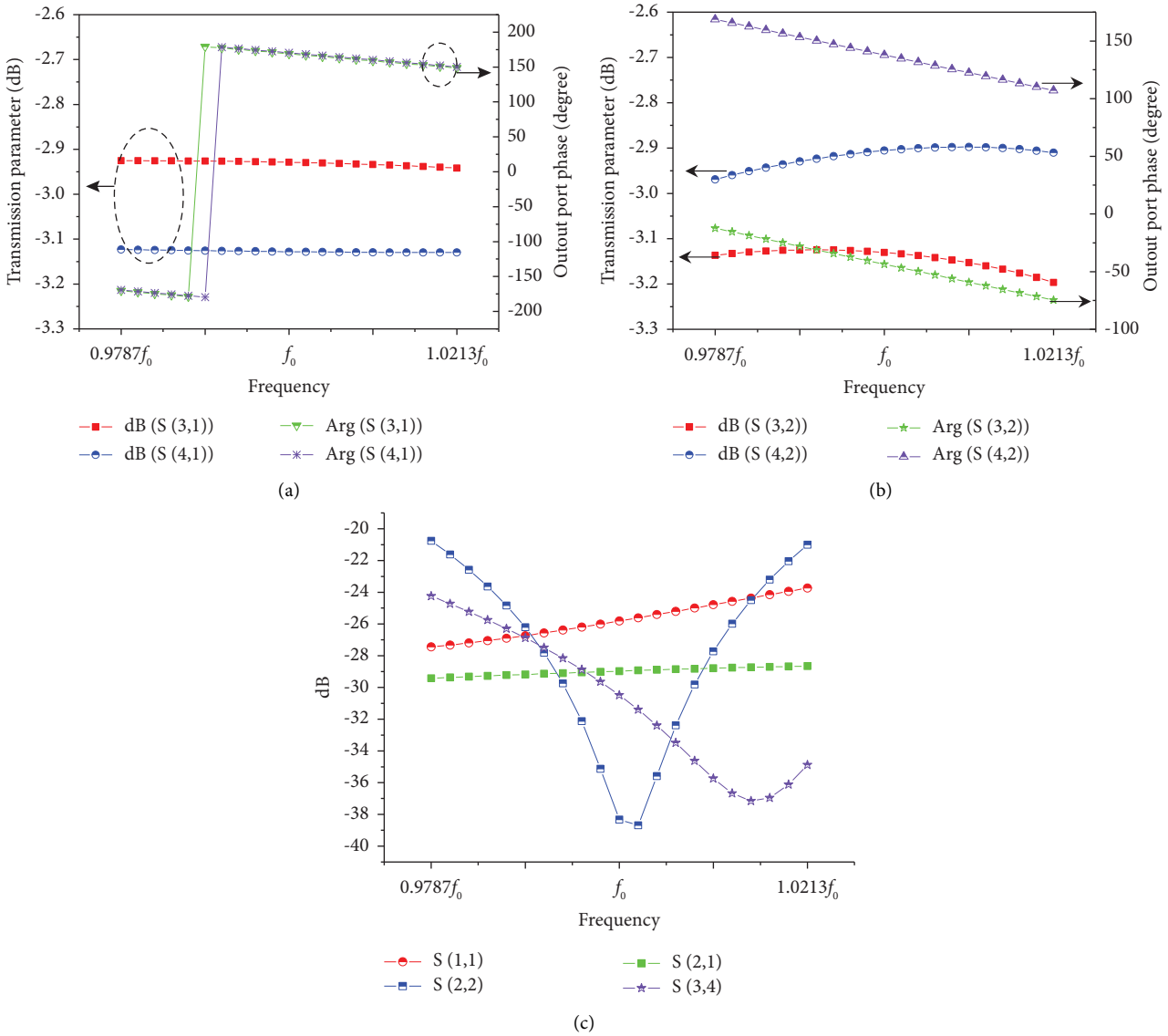

Figure 12: Simulated results of QPMT: (a) transmission coefficients when incident at port 1, (b) transmission coefficients when incident at port 2, and (c) reflection and isolation characteristics.

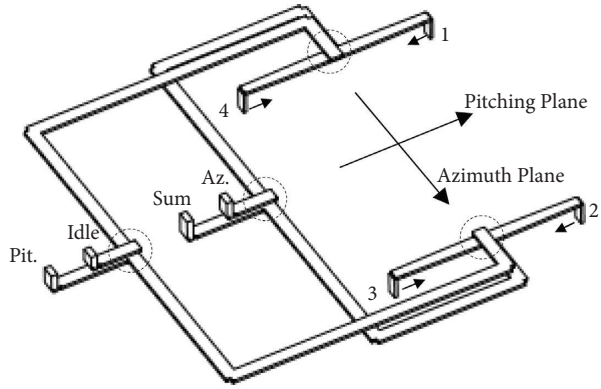

Figure 13: Comparator for the VP array.

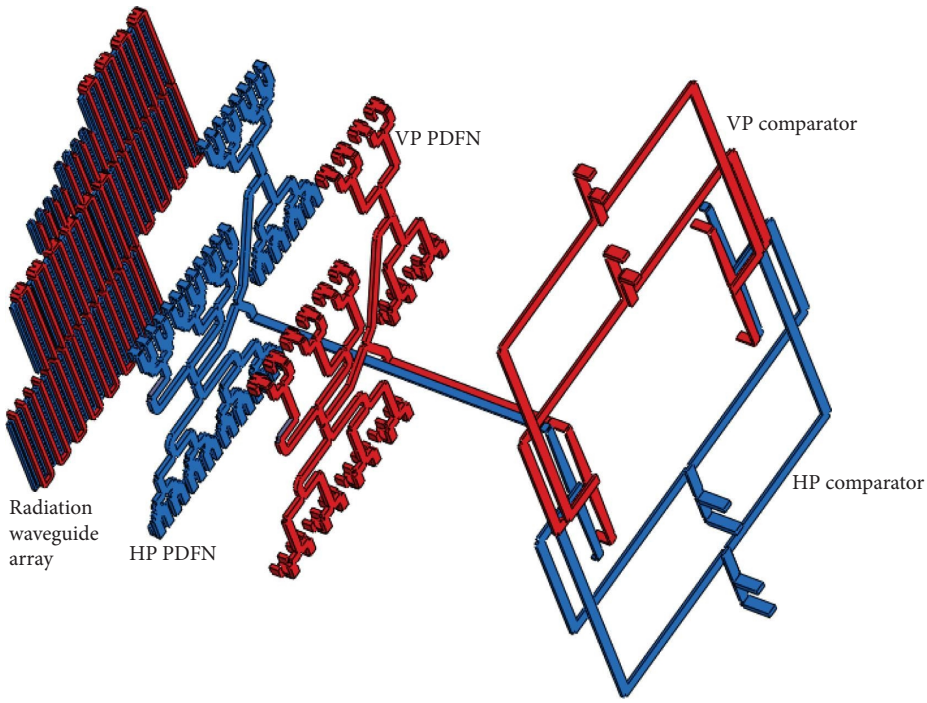

Figure 14: Split structure diagram of the monopole SWA.

a radar prototype, mainly to verify the distance detection ability of the dual polarization antenna for complex targets (with polarization rotation), and this task mainly relies on two polarized sum beams to complete. The radar prototype also needs to have a certain degree of direction-finding ability. In order to reduce receiver costs, only the pitch difference and azimuth difference beams of a single polarization are used. The horizontal polarization is selected, and the measured difference beams are shown in Figures 21(c) and 21(d).

The reflection coefficients of the antenna are measured with a vector network analyzer, and the results are shown in Figure 22; it can be seen that the reflection characteristic (less than −15 dB at most frequencies) of the HP is better than that of the VP; the reason is supposed to be that edge wall inclined slots of the VP slotted waveguide array are smaller than the broad wall longitudinal slots of the HP slotted waveguide array, so the VP slots are more difficult to machine and a small machining error has a greater impact on the antenna performance including reflection characteristics. It is very difficult to quantitatively determine the impact of machining errors on the antenna performance, but qualitatively speaking, the machining errors of the feeding network, especially the blockage caused by solder, will be clearly reflected in the reflection coefficient characteristics. The machining errors of the gaps affect not only the reflection coefficient but also the gain and side lobes, but have a relatively small impact on the 3 dB beam width.

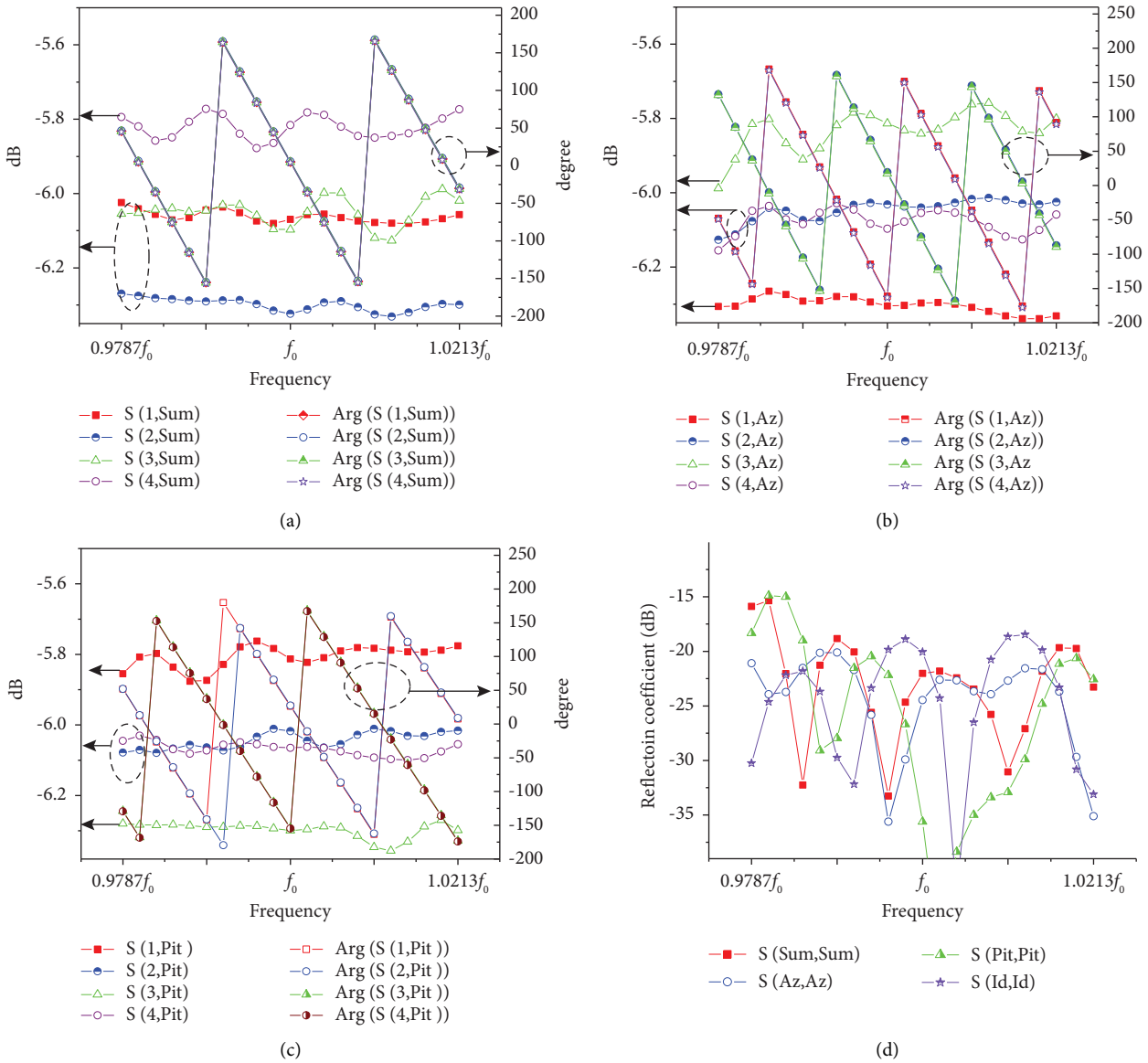

Figure 15: Characteristics of the comparator: (a) incident at port Sum, (b) incident at port Az., (c) incident at port Pit., and (d) reflection coefficient.

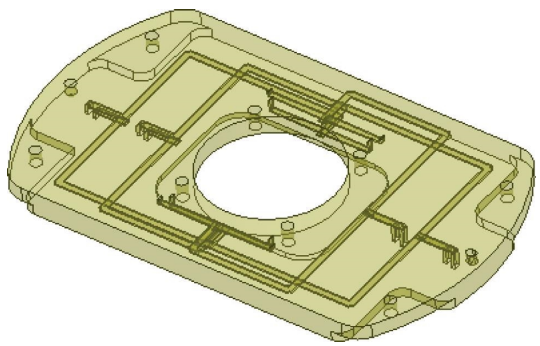

Figure 16: Comparator model.

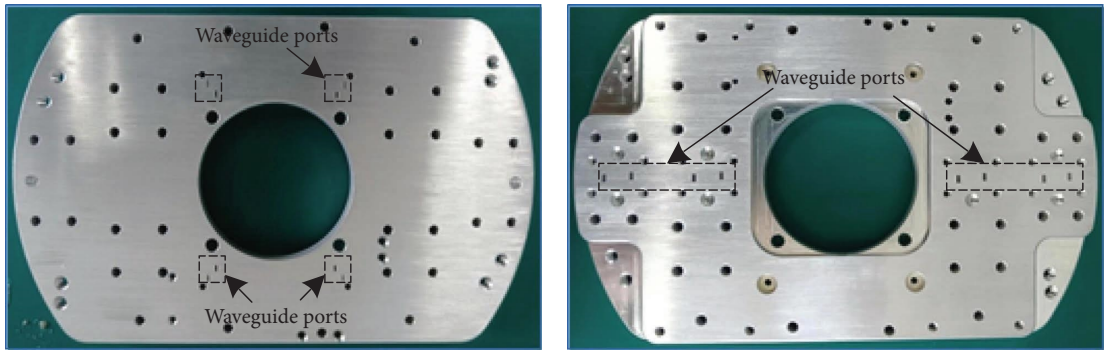

Figure 17: Manufactured comparator prototype: (a) interface to RF circuit and (b) interface to the slotted waveguide array.

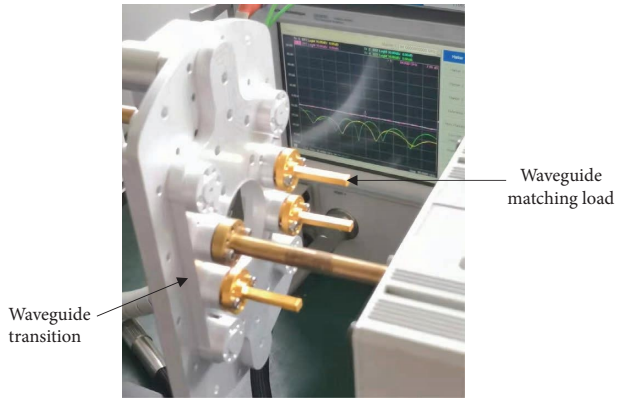

Figure 18: Testing environment.

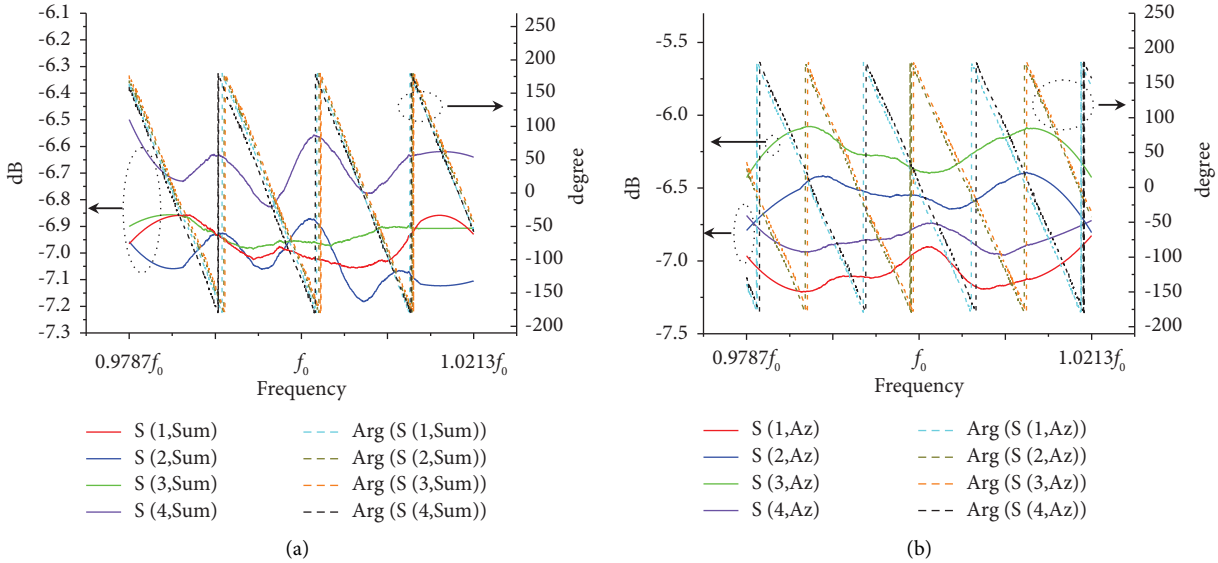

Figure 19: Continued.

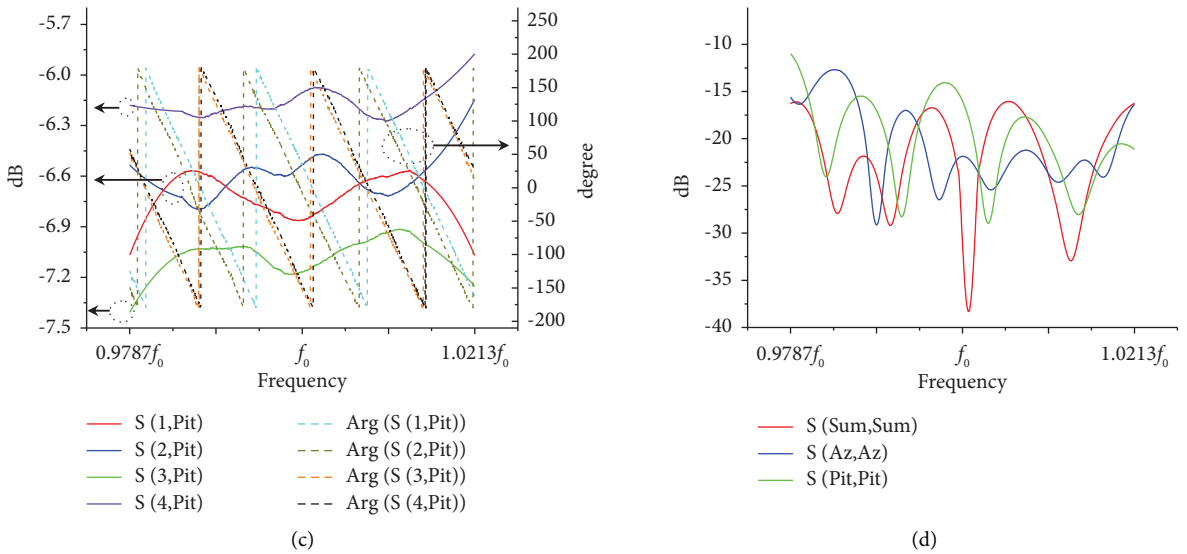

(c) (d)

Figure 19: Measured results of the comparator: (a) incident at port Sum, (b) incident at port Az., (c) incident at port Pit., and (d) reflection coefficient.

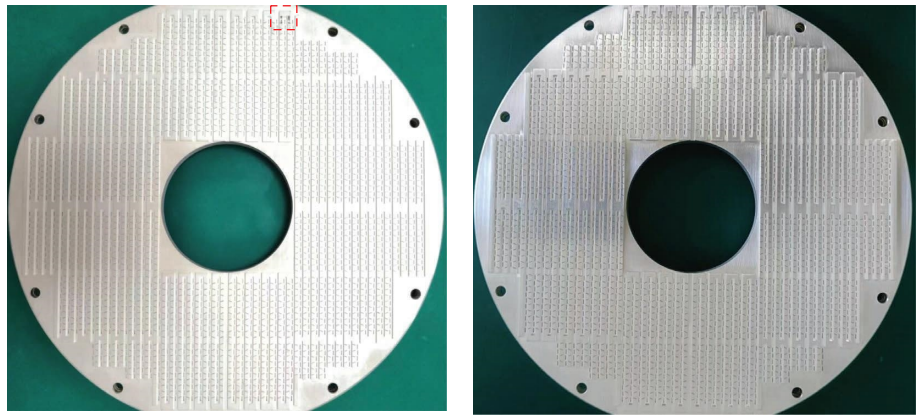

(a) (b)

Figure 20: Fabricated SWA: (a) antenna processed last time and (b) antenna processed this time.

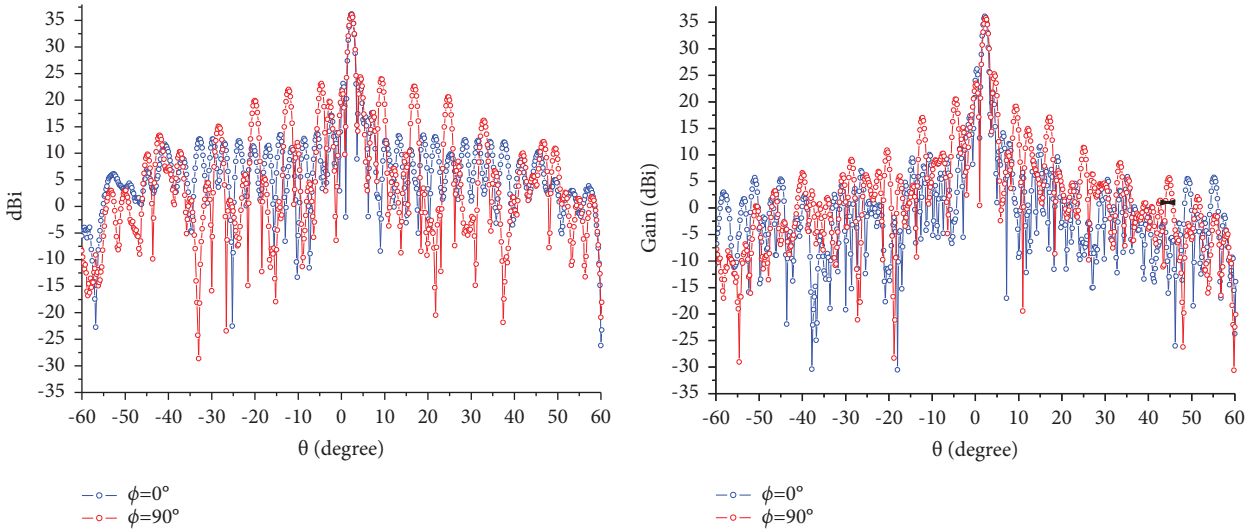

(a) (b)

Figure 21: Continued.

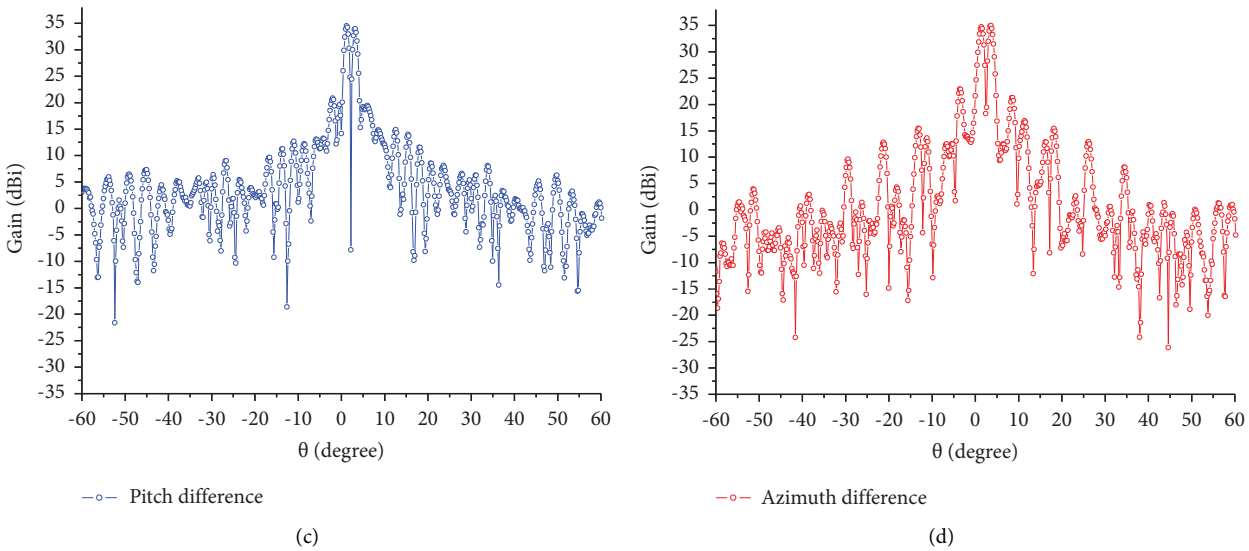

Figure 21: Measured results of the monopulse antenna: (a) sum beam of HP, (b) sum beam of VP, (c) pitch difference beam of HP, and (d) azimuth difference beam of HP.

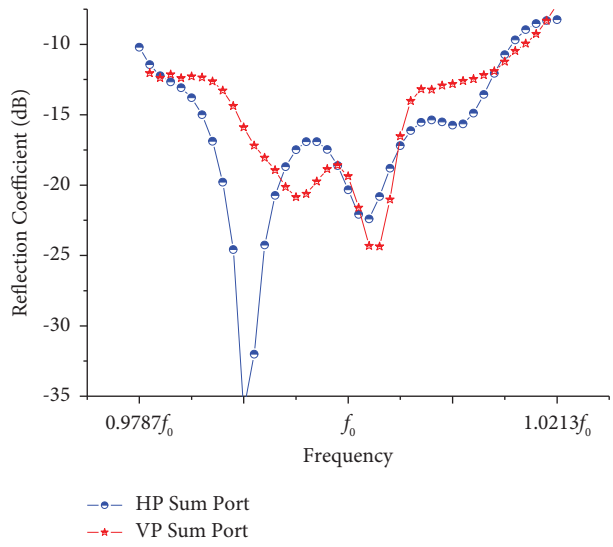

Figure 22: Reflection coefficients of the antenna.

4. Conclusion

A design of the monopulse feeding network for a dual polarization slotted waveguide array fabricated on an annular disk is presented in this paper. The monopulse feeding network of each polarization is composed of a power distribution network and a comparator. The power distribution network is irregular because the slotted waveguide array is arranged on an annular disk. The design details and simulation results of the several key components of the power distribution network are presented. Quasiplanar magic tees were designed and used to construct the compact sum and difference comparator. The antenna system consists of two comparators, which are used to generate sum and difference beams for horizontal polarization and vertical polarization, respectively. Finally, the monopulse slotted waveguide array antenna is divided into two modules, a comparator module and an antenna module (including the power distribution network) and fabricated with the layered processing and bonding process. Scattering parameters of the comparator are measured using the network analyzer, and the measured results agree with the simulated results. Screwing the comparator module and antenna module together, a monopulse slotted waveguide array antenna is obtained, and the sum beam and difference beam characteristics of the antenna are measured in a microwave chamber, which shows that the sum and difference performance of the antenna is satisfactory.

Data Availability

All data including key component parameters are given in the paper.

Conflicts of Interest

The authors declare that they have no conflicts of interest.

Acknowledgments

This work was supported in part by the Natural Science Foundation for Excellent Young Scholars of Jiangsu Province (Grant no. BK20220128) and the National Key R&D Program of China (Grant no. 2019YFE0120700). This work was also supported by Research Square https://www.researchsquare.com/article/rs-3214671/v1 [17].

References

[1] Y. H. Choung, K. R. Goudey, and L. G. Bryans, "Theory and design of a ku-band TE/sub 21/-mode coupler," *IEEE Transactions on Microwave Theory and Techniques*, vol. 30, no. 11, pp. 1862–1866, 1982.

[2] P. Magnusson, M. Di Salvo, and C. Scarchilli, "A dual polarised slotted waveguide antenna for satellite based wind scatterometer instruments," in *Proceedings of the 7th European Conference on Antennas and Propagation (EuCAP)*, pp. 3449–3452, Gothenburg, Sweden, April 2013.

[3] M. Skolnik, *Introduction to Radar Systems*, McGraw-Hill Science, New York, NY, USA, 2002.

[4] W. Wu, J. Yin, and N. Yuan, "Design of an efficient X-band waveguide-fed microstrip patch array," *IEEE Transactions on Antennas and Propagation*, vol. 55, no. 7, pp. 1933–1939, 2007.

[5] M. Shahabadi, D. Busuioc, A. Borji, and S. Safavi-Naeini, "Low-cost, high-efficiency quasi-planar array of waveguide-fed circularly polarized microstrip antennas," *IEEE Transactions on Antennas and Propagation*, vol. 53, no. 6, pp. 2036–2043, 2005.

[6] P. Sadri-Moshkenani, J. Rashed-Mohassel, and M. Shahabadi, "Microstrip antenna array fed by a low-loss gap-waveguide feed network," *IEEE Transactions on Antennas and Propagation*, vol. 66, no. 8, pp. 4359–4363, 2018.

[7] Z. Ding, S. Xiao, M.-C. Tang, and C. Liu, "A compact highly efficient hybrid antenna array for W-band applications," *IEEE Antennas and Wireless Propagation Letters*, vol. 17, no. 8, pp. 1547–1551, 2018.

[8] L. Josefsson and S. R. Rengarajan, *Slotted Waveguide Array Antennas*, SciTech Publishing, an imprint of The Institution of Engineering and Technology, London, United Kingdom, 2018.

[9] B. Liu, W. Hong, Z. Kuai et al., "Substrate integrated waveguide (SIW) monopulse slot antenna array," *IEEE Transactions on Antennas and Propagation*, vol. 57, no. 1, pp. 275–279, 2009.

[10] H. Wang, D.-G. Fang, and X. G. Chen, "A compact single layer monopulse microstrip antenna array," *IEEE Transactions on Antennas and Propagation*, vol. 54, no. 2, pp. 503–509, 2006.

[11] S. A. Khatami, J. Meiguni, A. Amn-e-Elahi, and P. Rezaei, "Compact via-coupling fed monopulse antenna with orthogonal tracking capability in radiation pattern," *IEEE Antennas and Wireless Propagation Letters*, vol. 19, no. 8, pp. 1443–1446, 2020.

[12] Z. Wang, Y. Wang, H. Zeqin, and C. Peng, "Design of W-band dual polarized slotted waveguide array antenna on an annular disk," *Journal of Infrared, Millimeter and Terahertz Waves*, vol. 44, no. 1-2, pp. 1–16, 2022.

[13] D. Nagaraju and Y. K. Verma, "A compact wideband planar magic tee for monopulse antenna array applications," *IEEE Microwave and Wireless Components Letters*, vol. 31, no. 5, pp. 429–432, 2021.

[14] W. WangJ. Jin et al., "Waveguide slotted antenna array with broadband, dual-polarization and low cross-polarization for X-band SAR applications," in *Proceedings of the IEEE International Radar Conference*, pp. 653–656, Arlington, VA, USA, May 2005.

[15] A. Derneryd and A. Lagerstedt, "Novel slotted waveguide antenna with polarimetric capabilities," in *Proceedings of the Geoscience and Remote Sensing Symposium (IGARSS)*, pp. 2054–2056, Florence, Italy, July 1995.

[16] P. Magnusson, M. Di Salvo, and C. Scarchilli, "A dual polarised slotted waveguide antenna for satellite-based wind scatterometer instruments," in *Proceedings of the 7th European Conference on Antennas and Propagation (EuCAP)*, pp. 3449–3452, Gothenburg, Sweden, April 2013.

[17] Z. Wang, Y. Wang, S. Zhu, and P. Chen, "Design of the monopulse feeding network of a slotted waveguide array on an annular disk," https://www.researchsquare.com/article/rs-3214671/v1.